OPEN

NPG Asia Materials (2016) 8, e331; doi:10.1038/am.2016.182
www.nature.com/am

ORIGINAL ARTICLE

Highly conductive and flexible fiber for textile electronics obtained by extremely low-temperature atomic layer deposition of Pt

Jaehong Lee[1,6], Jaehong Yoon[1,6], Hyun Gu Kim[2], Subin Kang[1], Woo-Suk Oh[3], Hassan Algadi[1], Saleh Al-Sayari[4], Bonggeun Shong[3], Soo-Hyun Kim[5], Hyungjun Kim[1], Taeyoon Lee[1] and Han-Bo-Ram Lee[2]

Thermal atomic layer deposition (ALD) of metal has generally been achieved at high temperatures of around 300 °C or at relatively low temperatures with highly reactive counter reactants, including plasma radicals and O_3, which can induce severe damage to substrates. Here, the growth of metallic Pt layers by ALD at a low temperature of 80 °C is achieved by using [(1,2,5,6-η)-1,5-hexadiene]-dimethyl-platinum(II) (HDMP) and O_2 as the Pt precursor and counter reactant, respectively. ALD results in the successful growth of continuous Pt layers at the low temperature without any reactive reactants owing to the low activation energy of the HDMP precursor for surface reactions. Because of the high reactivity of the precursor, the growth of a pure Pt layer is achieved on various thermally weak substrates, leading to the fabrication of high-performance conductive cotton fibers by ALD. A capacitive-type textile pressure sensor is successfully demonstrated by stacking elastomeric rubber-coated conductive cotton fibers perpendicularly and integrating them onto a fabric with a 7 × 8 array configuration to identify the features of the applied pressure, which can be effectively utilized as a new platform for future wearable and textile electronics.
NPG Asia Materials (2016) **8,** e331; doi:10.1038/am.2016.182; published online 25 November 2016

INTRODUCTION

Atomic layer deposition (ALD) has widely attracted considerable interest for various high technologies, such as semiconductor devices and display devices,[1–3] because of its superb ability to deposit ultrathin films with excellent controllability and conformality even on complex three-dimensional (3D) structures.[1–8] Based on these superior properties, ALD has been intensively studied for several applications. In particular, textile electronics using the ALD is one of the promising fields since several materials can be readily deposited at temperatures lower than 150 °C by ALD, leading to the effective functionalization of thermally fragile substrates such as plastics, cellulose papers and polymeric textiles.[9–12] Chen *et al.*[13] demonstrated hydrophobic silk fabrics with a high laundering durability and robustness due to a TiO_2 coating deposited by ALD. However, in the case of metal ALD, since temperatures as high as 300 °C are generally required to achieve successful deposition with the thermal energy of the precursor reactions, it is difficult to deposit conformal metal films onto thermally weak substrates using ALD, causing difficulties in a wide range of applications, including textile electronics.[14,15] To ensure successful metal ALD at low temperatures, ALD in which the precursor is combined with a plasma-generated radical as highly reactive counter reactants has been investigated; however, the high energy of the plasma causes degradation of substrates that do not have a high thermal stability and robustness under plasma conditions.[16–19] In addition, Dendooven *et al.*[20] investigated Pt ALD at low temperatures around 100 °C by using O_3 as a reactant with a (methylcyclopentadienyl)trimethylplatinum ($MeCpPtMe_3$) precursor. A significant reduction of the growth temperatures in the ALD can be achieved by using O_3 as a counter reactant; nevertheless, the use of O_3, which has a high reactivity, leads to several drawbacks, such as severe damage that can fully etch stable substrates—including graphite—and limitations in conformal deposition on complex 3D structures with high aspect ratios.[21–24] These negative effects of the previously reported metal ALD severely limit the application of metal ALD that require thermally fragile substrates, despite the low deposition temperatures, as such substrates, which are generally composed of polymeric materials, have not only poor durability against mechanical damage but also highly complex 3D structures.

Herein, we describe an effective ALD process for Pt achieved at temperatures as low as 80 °C using [(1,2,5,6-η)-1,5-hexadiene]

[1]School of Electrical and Electronic Engineering, Yonsei University, Seoul, Republic of Korea; [2]Department of Materials Science and Engineering, Incheon National University, Incheon, Republic of Korea; [3]Department of Chemistry, Chungnam National University, Daejeon, Republic of Korea; [4]College of Science and Arts at Sharurah, Promising Center for Sensors and Electronic Devices, Najran University, Najran, Saudi Arabia and [5]School of Materials Science and Engineering, Yeungnam University, Gyeongsan-si, Republic of Korea
[6]These authors contributed equally to this work.
Correspondence: Professor T Lee, School of Electrical and Electronic Engineering, Yonsei University, Yonsei-ro 50, Seodaemun-gu, Seoul 03722, Republic of Korea.
E-mail: taeyoon.lee@yonsei.ac.kr
or Professor H-B-R Lee, Department of Materials Science and Engineering, Incheon National University, 119 Academi-ro, Yeonsu-gu, Incheon 22012, Republic of Korea.
E-mail: hbrlee@inu.ac.kr
Received 2 June 2016; revised 23 September 2016; accepted 26 September 2016

dimethylplatinum(II) (HDMP) and O_2 as a precursor and counter reactant. The HDMP precursor exhibited a significantly lower activation energy of 22.6 kcal mol^{-1} for surface reactions than the $MeCpPtMe_3$ precursor due to its molecular geometries, leading to the high reactivity even without any reactive counter reactants at the low temperature. To the best of our knowledge, the report of the successful metal ALD at the low temperatures below 100 °C with only O_2 as a counter reactant has never been discussed. By using low-temperature ALD for Pt, highly conformal Pt layers were deposited onto various thermally weak substrates, such as a strand of hair, papers and cotton fibers, which enables the substrates to have excellent electrical properties. As a proof of concept, a high-performance capacitive textile pressure sensor was successfully fabricated by crossing two conductive cotton fibers coated with poly(dimethylsiloxane) (PDMS) perpendicularly. The textile pressure sensor provided high performances such as a high sensitivity, a high stability and an extremely low detection limit. In addition, large-area textile pressure sensor arrays with a 7×8 array configuration were realized on a fabric to recognize the spatial distribution of pressure by a simple sewing method, which can be useful for various advanced wearable and textile electronics.

MATERIALS AND METHODS

Low-temperature ALD

A commercial ALD chamber with a 4-inch capable stage was used for the study (Supplementary Figure S1). The HDMP precursor, which was synthesized and provided by TANAKA KIKINZOKU KOGYO.K.K (Supplementary Figure S2), was stored in a stainless steel canister, whose temperature was maintained at 50 °C to obtain an appropriate molecular supply during the ALD process. The HDMP canister was connected to the process chamber by one port, and vaporized HDMP molecules were transported by N_2 carrier gas. The counter reactant was O_2, and its flow was controlled by a mass-flow controller, which was supplied from a 99.99% O_2 cylinder. N_2 was used for both the carrier gas and purging gas, which also was controlled by mass-flow controller. The standard ALD process comprised four steps: precursor exposure (t_s), N_2 purging (t_p), reactant exposure (t_r) and purging. For better conformality and uniformity, an infiltration step was performed after the precursor and reactant exposure step.

Fabrication of textile-based pressure sensors

The conductive fibers produced by Pt ALD were located perpendicular to the ground on a stand with 100 g weights. Then, 1.5 ml of a PDMS solution, which was composed of a Sylgard 184 base and a curing agent with a weight ratio of 5:1 (base:curing agent), flowed along the conductive fibers at a constant flow rate of 0.5 ml s^{-1}. After a sufficient time had passed for the formation of a uniform layer of PDMS solution on the surface of the conductive fibers, the fibers were annealed at 80 °C for 2 h. Then, the two PDMS-coated conductive fibers were crossed perpendicularly.

Quantum chemical calculations

Density functional theory calculations were performed employing ORCA program suite.[25] The geometries were optimized using the hybrid-generalized gradient approximation (GGA) B3LYP-D3 functional with the def2-SVP basis set and the corresponding effective core potential for the Pt atom.[26] The single-point energies of the optimized geometries were obtained with double-hybrid-meta-GGA PWPB95-D3 functional with the zeroth-order regular approximation (ZORA) for relativistic effects and the zeroth-order regular approximation-TZVP (Ahlrichs' triple zeta valence basis set with an additional set of polarization functions, as defined in ref. 27) basis set for all atoms.[28–30] The RIJCOSX approximation was applied to all calculations to improve the computational speed.[31] The hydroxylated silica surface was modeled with a Si $(OH)_4$ cluster. The transition-state geometries were initially guessed and then confirmed after optimization to have a single imaginary vibrational frequency along the reaction coordinate.

Characterization

The surface morphologies were examined using a JEOL JSM-7001F field emission scanning electron microscope (SEM). The microstructure of the ALD Pt films was analyzed by using X-ray diffraction (Ultima IV, Rigaku, Tokyo, Japan). The apparent coverage was computationally calculated using ImageJ software from SEM plan-view images. Chemical composition analysis was performed using X-ray photoelectron spectroscopy (K-ALPHA, Thermo Fisher Scientific, Waltham, MA, USA), and the resistivity of the Pt layer was measured using a four-point probe system. The durability of the conductive cotton fiber under a bending test was measured using a customized bending machine. The weight fraction of Pt in the conductive fiber was evaluated using a thermogravimetry analysis (Q50, TA Instruments, New Castle, DE, USA). The capacitance of the pressure sensor was measured at a frequency of 300 kHz with a 1 V AC signal by using an Agilent (Santa Clara, CA, USA) E4980A, Precision LCR Meter. The mechanical force and its frequency for the measurement of the sensing performance were controlled by a universal manipulator (Teraleader, Daejeon, Republic of Korea).

RESULTS AND DISCUSSION

To investigate the deposition of Pt film by ALD with an HDMP precursor, the saturation behavior and self-limiting surface reactions of the ALD were verified by measuring the growth per cycles (GPCs) of the deposited Pt according to the precursor and counter-reactant exposure time as shown in Figure 1a. The deposition process for Pt was carried out using HDMP and O_2 gas as a precursor and counter reactant, respectively, at 300 °C. The GPCs of the deposited Pt were saturated at a precursor exposure time of 2 s and reactant exposure time of 4 s, indicating that the deposition of Pt was achieved in a self-limiting surface reaction mode of ALD. To compare the deposition characteristics of the HDMP precursor with a $MeCpPtMe_3$ precursor, which is widely used for the ALD of Pt, the apparent coverage of Pt deposited on a SiO_2/Si substrate by ALD was examined for incremental ALD cycles as shown in Figure 1b. Although the apparent coverage of the Pt film by ALD with the $MeCpPtMe_3$ precursor reached 100 % at around 400 cycles, the surface coverage of the Pt film deposited using the HDMP precursor exhibited a significantly rapid increase of surface coverage in a low cycle region and reached a plateau at around 100 cycles, indicating that the HDMP precursor adsorbed far more actively on the surface, leading to faster nucleation than $MeCpPtMe_3$.

For a more quantitative analysis, an isothermal nucleation and growth model that was used in our studies regarding Pt nanoparticles was adopted for both precursors.[32] According to the isothermal model based on nucleation incubation, the surface coverage of deposited Pt can be calculated as follows:

$$\frac{A}{A_0} = 1 - exp\ (-A_0 \int_0^t I_o e^{-\frac{\tau_I}{\tau}} \pi\ (\nu(t-\tau))^2 d\tau), \quad (1)$$

where A and A_0 are the total area covered by the deposited Pt and the area of the substrate, respectively; t is the number of ALD cycles with the steady-state nucleation rate I_o; and the GPCs of the Pt film ν is defined by thickness per an ALD cycle and the nucleation incubation time τ_I. The apparent coverage data calculated by the isothermal model are represented by solid lines in Figure 1b, exhibiting excellent agreement with the experimental results, with correlation coefficients (R_2) of 0.991 and 0.997 for the $MeCpPtMe_3$ and HDMP precursors, respectively. Important variables, including the steady-state nucleation rate (I_o) and the nucleation incubation time (τ_I), were determined from the calculation based on the theoretical model, as shown in Table 1. The steady-state nucleation rate (I_o) of Pt ALD for the HDMP precursor was far faster (eight times) than that for the $MeCpPtMe_3$ precursor, inducing a rapid increase of nucleation sites. In addition,

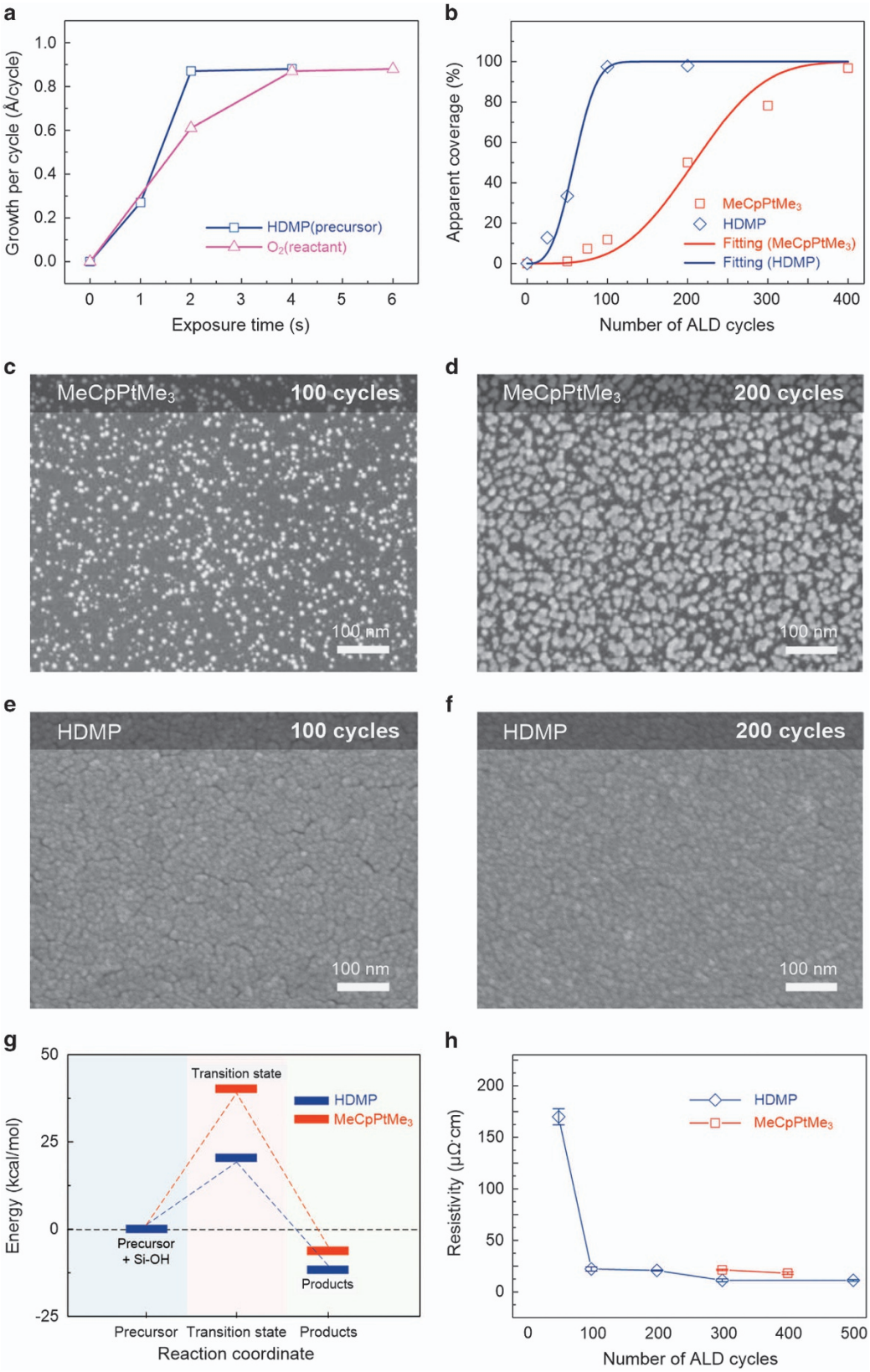

Figure 1 (**a**) GPCs of Pt films according to the exposure time of the precursor and counter reactants during the ALD process. HDMP and O_2 gas were used as the precursor and counter reactant, respectively, for the ALD of Pt. (**b**) Apparent coverage of the Pt films deposited by ALD using the $MeCpPtMe_3$ (blue) and HDMP (red) precursors. The solid lines indicate the corresponding fitting results for the nucleation model. (**c**–**f**) Typical SEM images showing the Pt deposited via ALD using the $MeCpPtMe_3$ precursor (**c**, **d**) and the HDMP precursor (**e**, **f**) at 100 and 200 cycles. (**g**) Density functional theory-calculated energies of the critical points along the reaction coordinate for the adsorption of the two precursors. (**h**) Electrical resistivity of the Pt films deposited by ALD according to the number of ALD cycles.

Table 1 Fitting parameters based on the isothermal nucleation model

Precursors	R^{2a}	I_o^b	τ_I [s]^c
$MeCpPtMe_3$	0.99112	0.56×10^{-4}	21
HDMP	0.99685	4.07×10^{-4}	8.97×10^{-7}

Abbreviations: HDMP, [(1,2,5,6-η)-1,5-hexadiene]dimethylplatinum(II); $MeCpPtMe_3$, (methylcyclopentadienyl)trimethylplatinum.
[a]Correlation coefficient related to the agreement between experimental results and theoretical model.
[b]Steady-state nucleation rate for Pt in ALD.
[c]Nucleation incubation time for Pt in ALD.

there was hardly any nucleation incubation time (τ_I), which is defined as the time needed to form surface species for Pt nucleation, for the HDMP precursor despite the long nucleation incubation time of 21 cycles for the $MeCpPtMe_3$ precursor. These results show that the ALD for Pt based on the HDMP precursor has an excellent efficiency with regard to the nucleation of Pt compared with the $MeCpPtMe_3$ precursor. Figure 1c–f show typical SEM images of Pt deposited on SiO_2/Si substrates using the $MeCpPtMe_3$ and HDMP precursors at 300 °C with 100 and 200 cycles. As shown in the SEM images, the Pt ALD using the HDMP precursor achieved a high surface coverage close to a continuous film, whereas the Pt deposition using the $MeCpPtMe_3$ precursor yielded a morphology of island growth in the same cycles of the ALD process. In addition, to compare ALD Pt deposited by using other precursors, the X-ray diffraction spectra were measured from ALD Pt films on SiO2 substrates using the HDMP precursors and O2 counter reactants at various deposition temperatures of 200, 250 and 300 °C, as shown in Supplementary Figure S3. For all the Pt films deposited with various growth temperatures, the X-ray diffraction results show a metallic Pt(111) diffraction peak at 40.013°, which corresponds to the formation of the metallic Pt(111) crystal plane,[23] indicating that the ALD Pt films with the HDMP precursor have a polycrystalline microstructure, similar to Pt films deposited with other Pt precursors.

The adsorption mechanism of the Pt precursor in the ALD was investigated by density functional theory calculations (Figure 1g). The reactions of the precursor with the silanol moiety of the hydroxylated silica surface, resulting in the elimination of CH_4 and the adsorption of the rest were considered.[33] The activation energy for such surface reaction of HDMP (22.6 kcal mol^{-1}) was significantly lower than that of $MeCpPtMe_3$ (40.8 kcal mol^{-1}), which is consistent with experimental observations. The difference between the energetics of the two precursors can be attributed to their molecular geometries. The transition states of both precursors assume a square pyramidal geometry that imposes steric repulsion between the ligands, as described in Supplementary Figure S4. Although the binding configuration of η^4-1,5-hexadinene for HDMP is similar for both the molecular precursor and the transition state, η^5-MeCp of $MeCpPtMe_3$ suffers a large hindrance upon the fifth coordination to Pt and becomes η^1 in the transition state, losing its aromaticity and thus exhibiting a larger endothermicity. On the other hand, the adsorption energy of the CH_4-eliminated Pt fragments was only marginally more exothermic for HDMP (−11.1 kcal mol^{-1}) than for $MeCpPtMe_3$ (−6.3 kcal mol^{-1}), which is expected because the same bonds were cleaved (Pt-C and O-H) and formed (Pt-O and C-H) in either reaction. Therefore, the far higher nucleation rate and shorter nucleation incubation period of HDMP compared with $MeCpPtMe_3$ are explained by the intrinsically higher reactivity of the HDMP molecule upon dissociative adsorption.

Figure 1h shows the electrical properties of the Pt films deposited using both precursors according to the number of cycles in the ALD process. Although a low electrical resistivity of 16.3 μΩ·cm was achieved at 400 cycles in the case of the Pt film grown with the $MeCpPtMe_3$ precursor, the deposited Pt film was not electrically conductive under 300 cycles, indicating the poor continuity of the film at the deposition conditions as shown in Figure 1c and d. The electrical resistivity of the Pt film deposited using the HDMP precursor was significantly reduced to 11.2 μΩ·cm, which is comparable to the bulk resistivity of Pt (10.5 μΩ·cm),[17] at 400 cycles and even exhibited excellent electrical properties under the poor condition of 100 cycles. For metal ALD, undesired effects such as nucleation delay or island growth, which hinder a high conformality and the thickness control of the deposited metal film, can occur frequently. These are mainly due to the high surface energy of the metal, which can lead to the low wettability of the metal and agglomeration into metal islands during the ALD process. Therefore, in metal ALD, it is generally difficult to control the thickness of the film and achieve a continuous film when a thin film with a thickness of a few nanometers is desired. Nevertheless, the Pt film grown by Pt ALD using the HDMP precursor exhibited a resistivity of 170 μΩ·cm in 50 cycles, as shown in Figure 1f, indicating that a continuous Pt film was successfully achieved through ALD using the HDMP precursor, although the film are very thin, having a thickness of 4 nm.

To verify the high reactivity of the HDMP precursor for Pt ALD with regard to the growth temperature, the deposition of the Pt film was investigated for various growth temperatures. Figure 2a shows the GPCs of the Pt films on SiO_2/Si substrates obtained by ALD with the two precursors as a function of the deposition temperature. The GPCs of the Pt films deposited using the HDMP and $MeCpPtMe_3$ precursors were measured as 0.88 and 0.54 Å per cycle, respectively, in their ALD windows (HDMP precursor: 250–300 °C, $MeCpPtMe_3$ precursor: 275–300 °C), confirming the high reactivity of the HDMP precursor. The HDMP precursor, in particular, yielded the successful deposition of Pt even at a temperature as low as 80 °C, at which ALD for Pt using the $MeCpPtMe_3$ precursor and O_2 as a counter reactant was not achieved. As described in Figure 2b, based on the superb efficiency of the HDMP precursor for depositing Pt at a low temperature, the Pt film deposited at the low temperature (80 °C) had a high electrical performance of 172 μΩ·cm, which is related to the excellent continuity of the film, despite the use of O_2 gas as a counter reactant instead of O_3 gas or plasma treatment. To evaluate the quality of the deposited Pt film, films deposited using the HDMP precursor at 100 and 300 °C were characterized by X-ray photoelectron spectroscopy, as shown in Figure 2c. The two peaks in the Pt core-level energy region of the X-ray photoelectron spectroscopy spectra described in Figure 2c are characterized by metallic Pt $4f_{7/2}$ (71 eV) and $4f_{5/2}$ (74.2 eV). There is no considerable deconvolution of the peaks, owing to the formation of PtO_x (72.3, 73.8 eV), indicating that the deposited Pt film has a high purity despite the low deposition temperature. Since it is difficult to successfully deposit Pt films at low temperatures by ALD with the $MeCpPtMe_3$ precursor and O_2 counter reactants, low-temperature ALD for high-purity Pt films using the HDMP precursor and a stable counter reactant (O_2 gas) can be effectively applied to coat conformal Pt layers on thermally fragile substrates. Using the strong advantage of low-temperature ALD for Pt, Pt layers were successfully deposited onto the surfaces of various thermally weak substrates, including a strand of hair and a sheet of paper. As shown in the SEM images of Figure 2d–i, the Pt layers were conformally deposited onto the surfaces of the substrates without any remarkable destruction of the structure, despite their poor thermal stability.

To demonstrate the ability of the low-temperature ALD, highly conductive fibers were successfully fabricated by depositing Pt layers

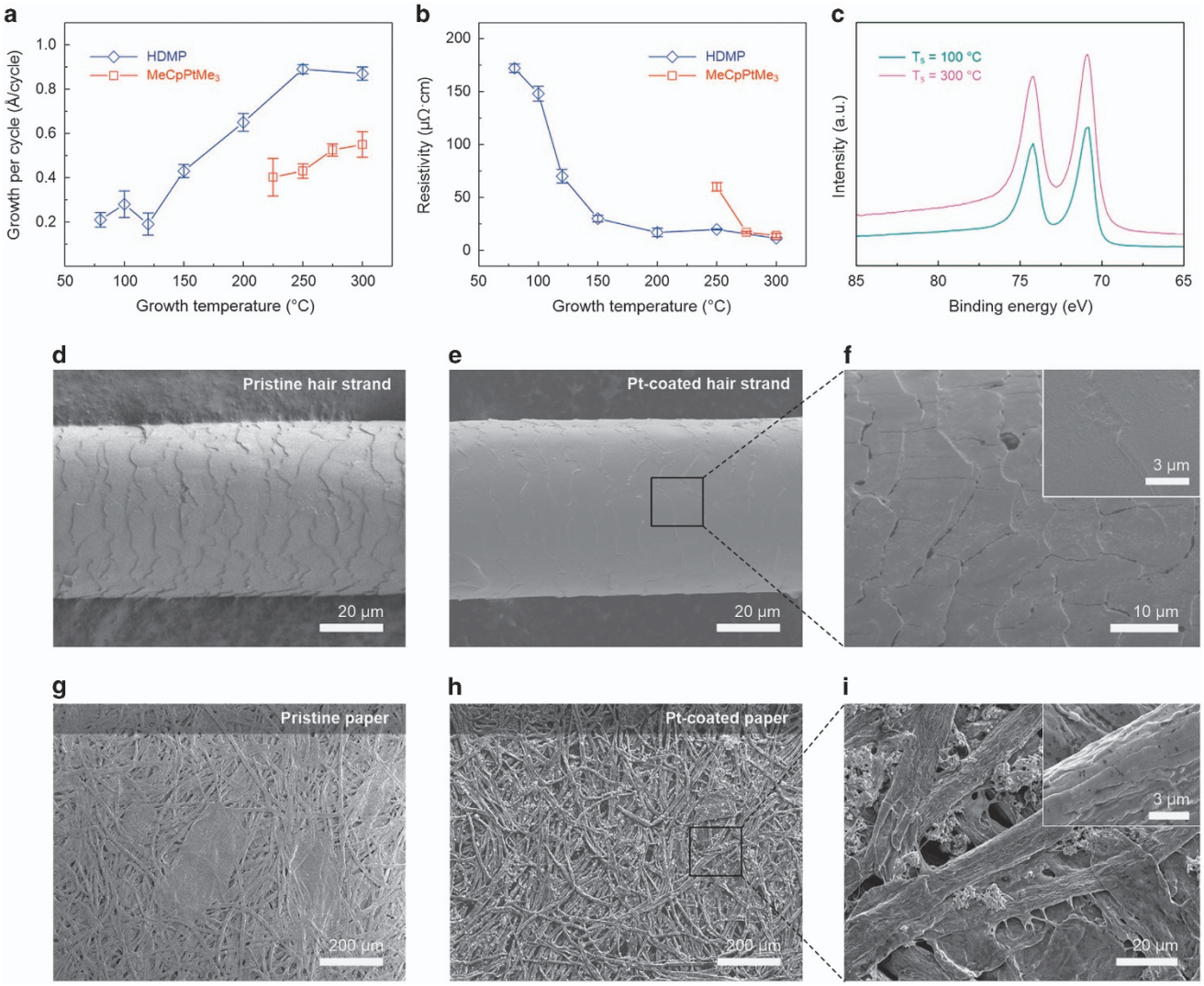

Figure 2 (**a**–**b**) GPCs (**a**) and electrical resistivity (**b**) of the Pt films according to the growth temperatures during the ALD process with respect to the two precursors. (**c**) X-ray photoelectron spectroscopy spectra of Pt films grown by ALD with the HDMP precursor at the temperatures of 100 and 300 °C. (**d**) SEM image of the surface of a pristine hair strand. (**e**–**f**) SEM images of a Pt-coated hair strand (**e**) after ALD at low temperatures and a corresponding higher-magnification image (**f**) (inset shows a far higher-magnification SEM image of **f**). (**g**) SEM image showing the complex 3D surface of pristine paper. (**h**–**i**) SEM images of the surface of Pt-coated paper (**h**) and corresponding higher-magnification images (**i**).

onto the surfaces of cotton fibers, which are the most frequently used textile in the related industry, through ALD with the HDMP precursor. Various conductive fibers using carbon-based material and metal material have been intensively studied for its promising applications such as sensors, organic displays and energy storage devices.[34–36] As shown in Figure 3a, the original cotton fiber had a complex 3D structure owing to its twisted structure of yarns and comprised mostly cellulose, which is a thermally weak polymeric material. Nevertheless, conformal Pt layers were successfully deposited onto the entire surface of the cotton fiber by ALD without any considerable damage to the fiber, as shown in the SEM images of Figure 3b and c. The energy dispersive spectroscopy mapping image of the conductive cotton fiber shows that the Pt layer was uniformly deposited onto the surface of the 3D structure of the conductive fiber through ALD using the HDMP precursor (Supplementary Figure S5). Figure 3d provides a photograph of the conductive cotton fiber coated with the Pt layer and the untreated cotton fiber, showing that the surface color of the conductive cotton fiber was changed to gray owing to the conformally deposited Pt layer. Because of the highly effective Pt coating through the ALD, the Pt layer deposited on the cotton fiber maintained its continuity and conformality regardless of the number of ALD cycles (Supplementary Figure S6), and the conductive cotton fiber exhibited excellent electrical properties. Figure 3e displays the electrical resistance per unit length ($\Omega\,cm^{-1}$) of the conductive cotton fiber, indicating that the electrical resistance was reduced to $2.72\,\Omega\,cm^{-1}$ by increasing the number of cycles. Although the thickness of the Pt layers deposited on the cotton fiber may increase linearly as a function of the number of cycles, the electrical resistance of the conductive cotton fiber was inversely proportional to the square of the number of cycles. This is because the cross-sectional area of the Pt layers deposited on the cotton fiber, which is inversely proportional to the electrical resistance of the conductive fiber, is proportional to the square of the thickness of the Pt layers. According to the results, conductive cotton fibers with the desired electrical resistance can be fabricated by modulating the number of ALD cycles and can be applied to easily turn on a light-emitting diode easily (Supplementary

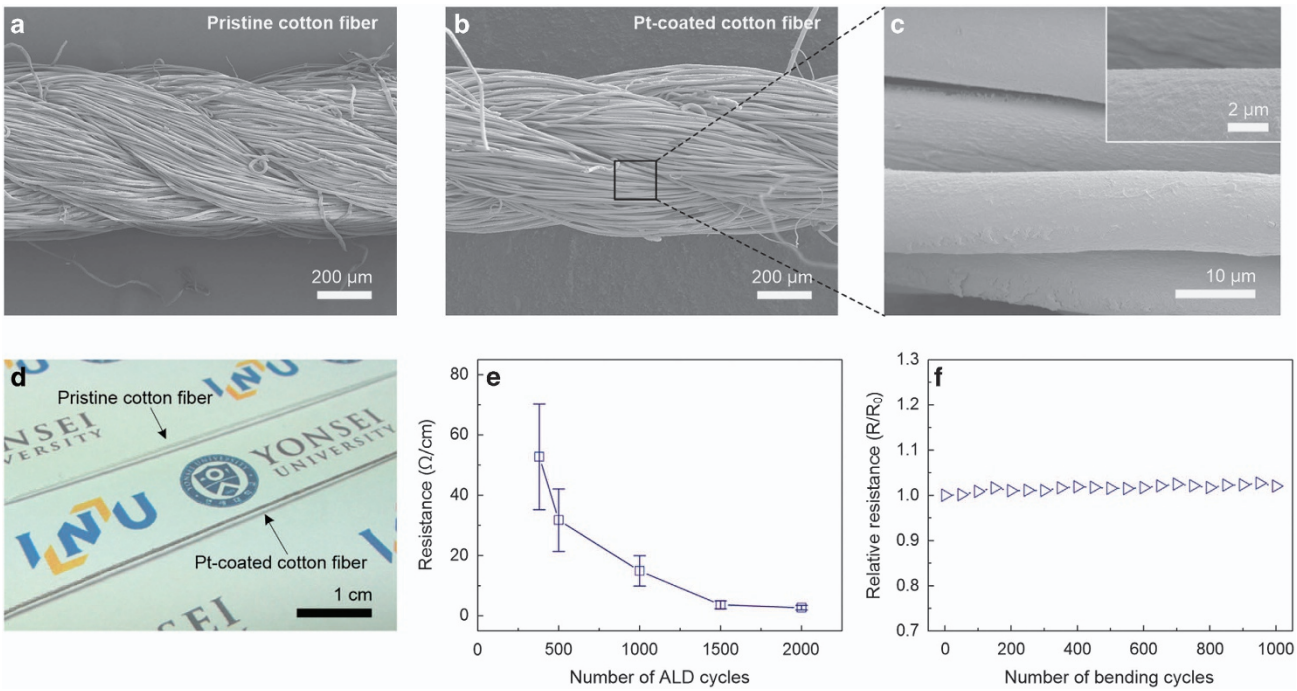

Figure 3 (**a**) Plain-view field emission scanning electron microscope image of the complex 3D structures of the pristine cotton fiber. (**b**–**c**) SEM images showing the surface of Pt-coated cotton fiber obtained by ALD at low temperatures (**b**) and a corresponding higher-magnification SEM image (**c**). The inset in (**c**) shows a far higher-magnification SEM image. (**d**) Photograph of the pristine cotton fiber and Pt-coated cotton fiber obtained by ALD. (**e**) Electrical resistance change of the Pt-coated conductive cotton fiber with respect to the number of ALD cycles. (**f**) Change in the relative electrical resistance of the conductive cotton fiber during the 1000-cycle bending test.

Figure S7 and Video 1). Figure 3f provides the excellent electrical stability of the conductive cotton fiber under a repeated bending test of 1000 cycles, which involved bending deformation with a bending radius of 3 mm and the unfolding of the back of the fiber. Despite the intensive repeated cycles of folding deformation, the electrical resistance of the conductive cotton fiber was slightly increased by only 2.03 % (16.71–17.05 $\Omega\,cm^{-1}$), indicating the high stability of the conductive cotton fiber. The high stability under repeated external stimulations is attributed to the excellent conformality and continuity of the Pt layers deposited on the surfaces of the complex 3D structures of the cotton fibers. In addition, thermogravimetric analysis measurements, which provide weight-content information about the Pt components in the conductive cotton fiber, were conducted as shown in Supplementary Figure S8. The weight content of Pt in the conductive cotton fiber was measured as 8.91–17.87 wt%, which is far smaller than that in previously reported metal-based conductive fibers (60–85 wt%).[37,38] The very small weight content of Pt in the conductive cotton fiber, despite the excellent electrical performance, is mainly attributed to the ultrathin and conformal Pt layer deposited by ALD and enables the conductive cotton fiber fabricated by low-temperature Pt ALD to have a strong advantage regarding cost-effectiveness, as only an ultrasmall amount of noble metal is needed to fabricate the conductive fiber.

To demonstrate the ability of conductive cotton fiber to be applied to textile electronics, a high-performance textile pressure sensor was fabricated by crossing the Pt ALD conductive fibers after a PDMS layer was coated on the surface of the conductive fibers, as shown in Figure 4a. The PDMS layer uniformly covered the conductive fibers after the PDMS solution flowed along the vertical conductive fibers perpendicular to the ground and the samples were cured. After the crossing of the two PDMS-coated conductive fibers, a capacitive pressure sensor was built at the cross point of the fibers where the two conductive cotton fibers act as electrodes and the PDMS layer coated on the conductive fibers functioned as an elastic dielectric layer of the capacitor, as shown in the schematic of Figure 4a. Since PDMS has been generally used as an elastic dielectric material in capacitive pressure sensors for artificial skin owing to its outstanding elastic properties, the capacitance generated between the two conductive fibers at the cross point can be changed by the thickness change of the elastic dielectric layer induced by the applied pressure. To examine the ability of the textile pressure sensor to respond to external pressure, the capacitive responses ($\Delta C/C_o$) of the textile pressure sensor to applied loads of 0.1, 0.5 and 1 N were examined, as shown in Figure 4b. The pressure sensor had stable responses despite the successive loading and unloading of the various loads, confirming its reliability. In addition, the textile pressure sensor exhibited a rapid change in the capacitive response against progressively increasing force applied to the sensor, indicating its high sensitivity, as shown in Figure 4c. The high sensitivity of the textile pressure sensor results from simultaneous changes in both the contact area of the two PDMS-coated conductive fibers and the thickness of the dielectric layer in the textile pressure sensor according to the increasing external pressure.[37] For typical capacitive pressure sensors, the related equation governing the capacitance of the sensors is provided by $C = \varepsilon_0\varepsilon_r(A/d)$, where ε_0 and ε_r refer to the space permittivity and relative dielectric constant of the dielectric material, respectively, A and d denote the area of the capacitor and the distance between the separated electrodes, respectively. The change in the distance between electrodes is mainly used to detect the applied pressure based on the thickness change of the elastomeric dielectric layer in general capacitive pressure sensors. However, when the external pressure compresses the textile pressure sensor, the thickness of the PDMS layer, which is directly

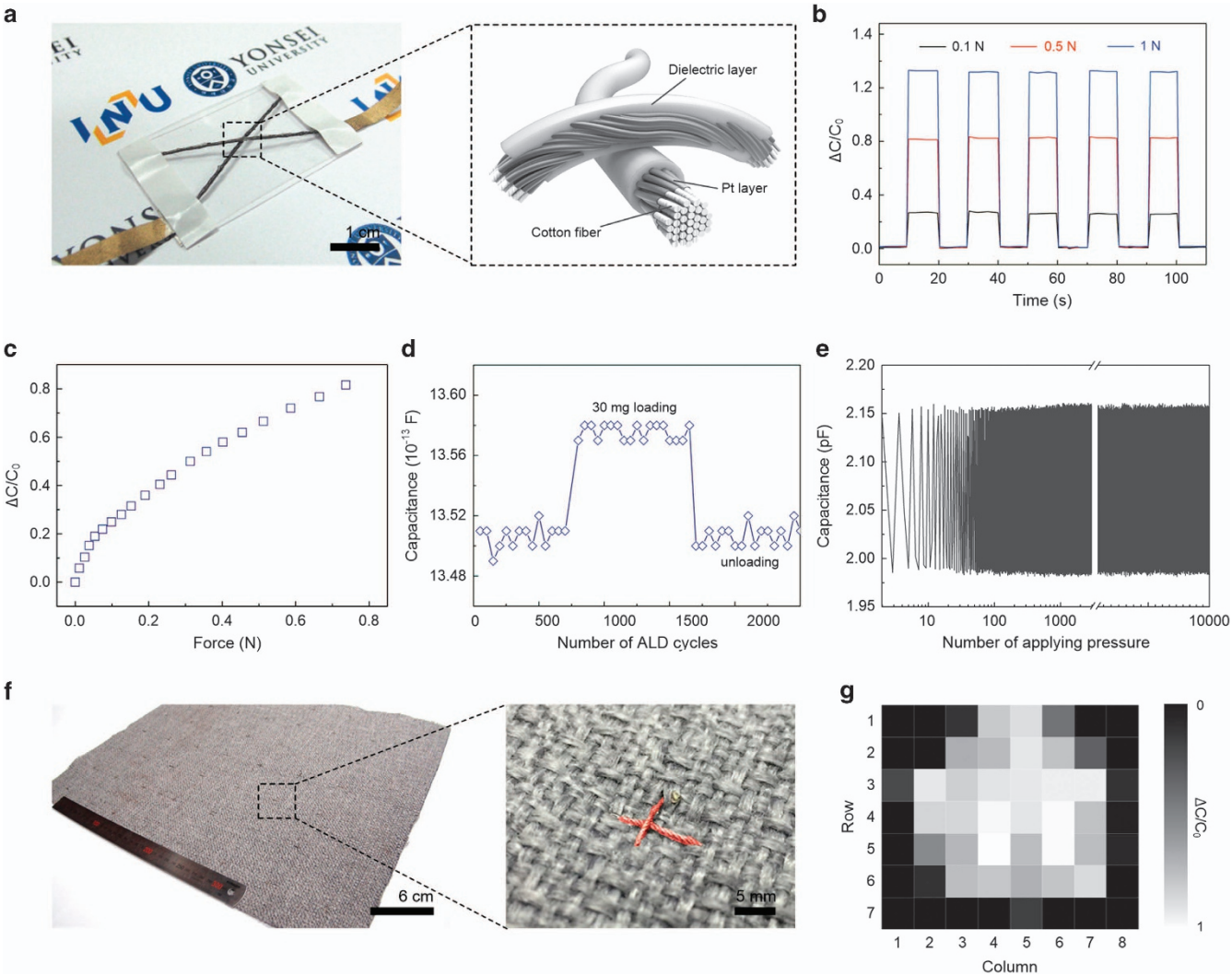

Figure 4 (**a**) Photograph of the fabricated textile pressure sensor based on Pt-coated conductive cotton fiber on a polyethylene terephthalate (PET) substrate and a corresponding schematic illustration of the pressure sensor. (**b**) Capacitive response of the textile pressure sensor to various loads of 0.1, 0.5 and 1 N. (**c**) Relative capacitance change with respect to the increasing applied load. (**d**) Capacitive response of the textile pressure sensor to the loading and unloading of a light weight (30 mg). (**e**) Stability of the textile pressure sensor under an applied load of 0.05 N for over 10 000 cycles. (**f**) Photographs of a textile-based pressure sensor array with a 7×8 configuration. (**g**) Capacitive-response mapping of the 56 pixel textile pressure sensor array for a sitter, where the bright regions correspond to the increased capacitance change of a pressure sensor.

related to the distance between electrodes, is reduced and the contact area between the two PDMS-coated conductive fibers, which is related to the area of the capacitor, is increased at the same time, resulting in a significant enhancement of the sensing performance. The decreasing slope in the graph described in Figure 4c, which indicates the sensitivity of the pressure sensor, in the higher applied-force regime above 0.1 N is attributed to the increase in the contact area of the sensor, inducing decrease of the effective stress applied on the contact area.[37] Based on the high performance of the textile pressure sensor, it was possible to reliably detect the placement and removal of an ultrasmall weight of around 30 mg, which is similar to the weight of a housefly, as shown in Figure 4d. The capacitive response of the textile pressure sensor was also found to be highly durable and reproducible against repeatedly applied pressures. Figure 4e exhibits the capacitive response of the textile pressure sensor under the repeated loading and unloading of an external load, indicating that the capacitance changes of the pressure sensor were stably maintained even under the intensive cycling test, which involved the loading and unloading of a load of 0.4 N for over 10 000 cycles.

As a proof of concept, a large-area 7×8 array configuration of the textile-based pressure sensors was fabricated on a cotton fabric with a total area of 50×40 cm by sewing the sensors, as shown in Figure 4f. Using a simple sewing method, numerous textile pressure sensors can be easily imbedded into any fabric as all-textile devices that can obtain spatial pressure information (Supplementary Figure S9). The smart fabric was used as a seat sensor to detect the spatial distribution of the applied pressure on the seat. In the case of vehicles, it is highly important to distinguish the features of a sitter, such as the body type, weight and presence of objects like a car seat. Figure 4g shows a capacitive-response mapping of the 56 pixel pressure sensor array against a sitter, where the bright regions correspond to the increased capacitance change of a pressure sensor. As demonstrated in Figure 4f–g, the smart fabric, including the pressure sensor array on a seat, detected the pressure distributions generated by the sitters (Supplementary Figure S10). In particular, owing to the high

performance of each pressure sensor in the array, the textile pressure sensor array on the fabric could successfully classify the body types of the sitters (Supplementary Figure S11). These results indicate that our textile pressure sensor fabricated using conductive cotton fibers exhibits significant potential to be used as an advanced occupant-classification system for vehicles. We expect the pressure sensors to be effectively utilized for various advanced wearable systems via the simple sewing method.

CONCLUSION

In summary, we developed a powerful ALD process for Pt that can be successfully achieved at temperatures as low as 80 °C and fabricated a highly conductive cotton fiber and textile pressure sensor using this Pt ALD process. Using an HDMP precursor with an unprecedented reactivity, Pt layers were conformally deposited on thermally fragile substrates by ALD at low growth temperatures. Using the highly conductive fibers prepared by Pt ALD, a high-performance capacitive textile pressure sensor was successfully fabricated. The textile pressure sensor exhibited a high sensitivity and excellent durability despite pressures repeatedly applied for 10 000 cycles. In addition, we demonstrated that the textile pressure sensor has enormous potential for realization of advanced e-textiles via the integration of multiple sensors onto a fabric in a large-area 7×8 array configuration to be utilized to an occupant-classification system that can identify the features of sitters. We believe that the textile pressure sensor and smart fabrics obtained through low-temperature Pt ALD are promising candidates for various wearable and smart fabric applications as a new platform for future textile electronics.

CONFLICT OF INTEREST

The authors declare no conflict of interest.

ACKNOWLEDGEMENTS

This research was supported by Basic Science Research Program through the National Research Foundation of Korea (NRF) funded by the Ministry of Education (2016R1D1A1B03935611) and the MOTIE (Ministry of Trade, Industry & Energy; 10053098) and KSRC (Korea Semiconductor Research Consortium) support program for the development of the future semiconductor device. This work was also supported by the Priority Research Centers Program (Grant No. 2009-0093823) through the National Research Foundation (NRF) of Korea funded by the Ministry of Education, Science and Technology (MEST), the R&D program of MOTIE/KEIT (Korea Evaluation Institute of Industrial Technology) [10064081, Development of fiber-based flexible multimodal pressure sensor and algorithm for gesture/posture-recognizable wearable devices], and the Ministry of Higher Education, Kingdom of Saudi Arabia for supporting this research through a grant (PCSED-009-14) under the Promising Centre for Sensors and Electronic Devices (PCSED) at Najran University, Kingdom of Saudi Arabia. We thank the TANAKA KIKINZOKU KOGYO.K.K. for helpful support of the Pt precursor.

1 King, J. S., Wittstock, A., Biener, J., Kucheyev, S. O., Wang, Y. M., Baumann, T. F., Giri, S. K., Hamza, A. V, Baeumer, M. & Bent, S. F. Ultralow loading Pt nanocatalysts prepared by atomic layer deposition on carbon aerogels. *Nano Lett.* **8**, 2405–2409 (2008).
2 Hyde, G. K., Park, K. J., Stewart, S. M., Hinestroza, J. P. & Parsons, G. N. Atomic layer deposition of conformal inorganic nanoscale coatings on three-dimensional natural fiber systems: effect of surface topology on film growth characteristics. *Langmuir* **23**, 9844–9849 (2007).
3 Christensen, S. T., Elam, J. W., Rabuffetti, F. A., Ma, Q., Weigand, S. J., Lee, B., Seifert, S., Stair, P. C., Poeppelmeier, K. R., Hersam, M. C. & Bedzyk, M. J. Controlled growth of platinum nanoparticles on strontium titanate nanocubes by atomic layer deposition. *Small* **5**, 750–757 (2009).
4 Jiang, X., Huang, H., Prinz, F. B. & Bent, S. F. Application of atomic layer deposition of platinum to solid oxide fuel cells. *Chem. Mater.* **20**, 3897–3905 (2008).
5 Yoneoka, S., Lee, J., Liger, M., Yama, G., Kodama, T., Gunji, M., Provine, J., Howe, R. T., Goodson, K. E. & Kenny, T. W. Electrical and thermal conduction in atomic layer deposition nanobridges down to 7 nm thickness. *Nano Lett.* **12**, 683–686 (2012).
6 Lin, Y.-H., Hsueh, Y.-C., Lee, P.-S., Wang, C.-C., Wu, J. M., Perng, T.-P. & Shih, H. C. Fabrication of tin dioxide nanowires with ultrahigh gas sensitivity by atomic layer deposition of platinum. *J. Mater. Chem.* **21**, 10552 (2011).
7 Knez, M., Nielsch, K. & Niinistö, L. Synthesis and surface engineering of complex nanostructures by atomic layer deposition. *Adv. Mater.* **19**, 3425–3438 (2007).
8 Schwartzberg, A. M. & Olynick, D. Complex materials by atomic layer deposition. *Adv. Mater.* **27**, 5778–5784 (2015).
9 Jur, J. S., Sweet, W. J., Oldham, C. J. & Parsons, G. N. Atomic layer deposition of conductive coatings on cotton, paper, and synthetic fibers: conductivity analysis and functional chemical sensing using 'all-fiber' capacitors. *Adv. Funct. Mater.* **21**, 1993–2002 (2011).
10 Hyde, G. K., McCullen, S. D., Jeon, S., Stewart, S. M., Jeon, H., Loboa, E. G. & Parsons, G. N. Atomic layer deposition and biocompatibility of titanium nitride nano-coatings on cellulose fiber substrates. *Biomed. Mater.* **4**, 025001 (2009).
11 Jur, J. S., Spagnola, J. C., Lee, K., Gong, B., Peng, Q. & Parsons, G. N. Temperature-dependent subsurface growth during atomic layer deposition on polypropylene and cellulose fibers. *Langmuir* **26**, 8239–8244 (2010).
12 Kemell, M., Pore, V., Ritala, M., Leskelä, M. & Lindén, M. Atomic layer deposition in nanometer-level replication of cellulosic substances and preparation of photocatalytic TiO_2/cellulose composites. *J. Am. Chem. Soc.* **127**, 14178–14179 (2005).
13 Chen, F., Yang, H., Liu, X., Chen, D., Xiao, X., Liu, K., Li, J., Cheng, F., Dong, B., Zhou, Y., Guo, Z., Qin, Y., Wang, S. & Xu, W. Facile fabrication of multifunctional hybrid silk fabrics with controllable surface wettability and laundering durability. *ACS Appl. Mater. Interfaces* **8**, 5653–5660 (2016).
14 Hämäläinen, J., Munnik, F., Ritala, M. & Leskelä, M. Atomic layer deposition of platinum oxide and metallic platinum thin films from Pt(acac) 2 and ozone. *Chem. Mater.* **20**, 6840–6846 (2008).
15 Lee, H.-B.-R., Pickrahn, K. L. & Bent, S. F. Effect of O_3 on growth of Pt by atomic layer deposition. *J. Phys. Chem. C* **118**, 12325–12332 (2014).
16 Longrie, D., Devloo-Casier, K., Deduytsche, D., Van den Berghe, S., Driesen, K. & Detavernier, C. Plasma-enhanced ALD of platinum with O_2, N_2 and NH_3 plasmas. *ECS J. Solid State Sci. Technol* **1**, Q123–Q129 (2012).
17 Knoops, H. C. M., Mackus, A. J. M., Donders, M. E., van de Sanden, M. C. M., Notten, P. H. L. & Kessels, W. M. M. Remote plasma ALD of platinum and platinum oxide films. *Electrochem. Solid-State Lett.* **12**, G34 (2009).
18 Baker, L., Cavanagh, A. S., Seghete, D., George, S. M., Mackus, A. J. M., Kessels, W. M. M., Liu, Z. Y. & Wagner, F. T. Nucleation and growth of Pt atomic layer deposition on Al203 substrates using (methylcyclopentadienyl)-trimethyl platinum and O_2 plasma. *J. Appl. Phys.* **109**, 084333 (2011).
19 Heo, J., Lee, S. Y., Eom, D., Hwang, C. S. & Kim, H. J. Enhanced nucleation behavior of atomic-layer-deposited Ru film on low-k dielectrics afforded by UV-O[sub 3] treatment. *Electrochem. Solid-State Lett.* **11**, G5 (2008).
20 Dendooven, J., Ramachandran, R. K., Devloo-Casier, K., Rampelberg, G., Filez, M., Poelman, H., Marin, G. B., Fonda, E. & Detavernier, C. Low-temperature atomic layer deposition of platinum using (methylcyclopentadienyl)trimethylplatinum and ozone. *J. Phys. Chem. C* **117**, 20557–20561 (2013).
21 Lee, H.-B.-R. & Bent, S. F. Formation of continuous Pt films on the graphite surface by atomic layer deposition with reactive O_3. *Chem. Mater.* **27**, 6802–6809 (2015).
22 Hämäläinen, J., Hatanpää, T., Puukilainen, E., Sajavaara, T., Ritala, M. & Leskelä, M. Iridium metal and iridium oxide thin films grown by atomic layer deposition at low temperatures. *J. Mater. Chem.* **21**, 16488 (2011).
23 Hämäläinen, J., Munnik, F., Ritala, M. & Leskelä, M. Study on atomic layer deposition of amorphous rhodium oxide thin films. *J. Electrochem. Soc.* **156**, D418 (2009).
24 Knoops, H. C. M., Elam, J. W., Libera, J. A. & Kessels, W. M. M. Surface loss in ozone-based atomic layer deposition processes. *Chem. Mater.* **23**, 2381–2387 (2011).
25 Neese, F. The ORCA program system. *Wiley Interdiscip. Rev. Comput. Mol. Sci.* **2**, 73–78 (2012).
26 Goerigk, L. & Grimme, S. Efficient and accurate double-hybrid-meta-GGA density functionals-evaluation with the extended GMTKN30 database for general main group thermochemistry, kinetics, and noncovalent interactions. *J. Chem. Theory Comput.* **7**, 291–309 (2011).
27 Weigend, F. & Ahlrichs, R. Balanced basis sets of split valence, triple zeta valence and quadruple zeta valence quality for H to Rn: Design and assessment of accuracy. *Phys. Chem. Chem. Phys.* **7**, 3297–3305 (2005).
28 Grimme, S., Antony, J., Ehrlich, S. & Krieg, H. A consistent and accurate ab initio parametrization of density functional dispersion correction (DFT-D) for the 94 elements H-Pu. *J. Chem. Phys.* **132**, 154104 (2010).
29 van Wüllen, C. Molecular density functional calculations in the regular relativistic approximation: method, application to coinage metal diatomics, hydrides, fluorides and chlorides, and comparison with first-order relativistic calculations. *J. Chem. Phys.* **109**, 392 (1998).
30 Pantazis, D. A., Chen, X.-Y., Landis, C. R. & Neese, F. All-electron scalar relativistic basis sets for third-row transition metal atoms. *J. Chem. Theory Comput.* **4**, 908–919 (2008).
31 Neese, F., Wennmohs, F., Hansen, A. & Becker, U. Efficient, approximate and parallel Hartree–Fock and hybrid DFT calculations. A 'chain-of-spheres' algorithm for the Hartree–Fock exchange. *Chem. Phys.* **356**, 98–109 (2009).

32 Lee, H.-B.-R., Mullings, M. N., Jiang, X., Clemens, B. M. & Bent, S. F. Nucleation-controlled growth of nanoparticles by atomic layer deposition. *Chem. Mater.* **24**, 4051–4059 (2012).
33 Kessels, W. M. M., Knoops, H. C. M., Dielissen, S. A. F., Mackus, A. J. M. & van de Sanden, M. C. M. Surface reactions during atomic layer deposition of Pt derived from gas phase infrared spectroscopy. *Appl. Phys. Lett.* **95**, 013114 (2009).
34 Peng, H., Sun, X., Cai, F., Chen, X., Zhu, Y., Liao, G., Chen, D., Li, Q., Lu, Y., Zhu, Y. & Jia, Q. Electrochromatic carbon nanotube/polydiacetylene nanocomposite fibres. *Nat. Nano* **4**, 738–741 (2009).
35 Chen, T., Qiu, L., Yang, Z., Cai, Z., Ren, J., Li, H., Lin, H., Sun, X. & Peng, H. An integrated 'energy wire' for both photoelectric conversion and energy storage. *Angew. Chemie Int. Ed.* **51**, 11977–11980 (2012).
36 Zhang, Z., Guo, K., Li, Y., Li, X., Guan, G., Li, H., Luo, Y., Zhao, F., Zhang, Q., Wei, B., Pei, Q. & Peng, H. A colour-tunable, weavable fibre-shaped polymer light-emitting electrochemical cell. *Nat. Phot.* **9**, 233–238 (2015).
37 Lee, J., Kwon, H., Seo, J., Shin, S., Koo, J. H., Pang, C., Son, S., Kim, J. H., Jang, Y. H., Kim, D. E. & Lee, T. Conductive fiber-based ultrasensitive textile pressure sensor for wearable electronics. *Adv. Mater.* **27**, 2433–2439 (2015).
38 Lee, S., Shin, S., Lee, S., Seo, J., Lee, J., Son, S., Cho, H. J., Algadi, H., Al-Sayari, S., Kim, D. E. & Lee, T. Ag nanowire reinforced highly stretchable conductive fibers for wearable electronics. *Adv. Funct. Mater.* **25**, 3114–3121 (2015).

Supplementary Information accompanies the paper on the NPG Asia Materials website (http://www.nature.com/am)